RAA 2018 Vol. **18** No. **8**, 104(14pp) doi: 10.1088/1674–4527/18/8/104

http://www.raa-journal.org *http://iopscience.iop.org/raa*

***R**esearch in*
***A**stronomy and*
***A**strophysics*

Analysis of the X-ray emission of OB stars: O stars

Elizaveta Ryspaeva[1,2] and Alexander Kholtygin[2]

[1] Main (Pulkovo) Astronomical Observatory, 196140 Saint Petersburg, Russia
[2] Saint Petersburg State University, 198504 Saint Petersburg, Russia; *afkholtygin@gmail.com*

Received 2017 November 30; accepted 2018 May 22

Abstract We investigate the global properties of X-ray emission from O stars, analyzing the X-ray spectra of 32 O stars from archival data of the *XMM-Newton* space observatory. We examine two hypotheses about of the origin of X-ray emission from O stars. The first is a paradigm proposed by Pollock, that was revealed from an analysis of the ζ Ori X-ray observation. The second is the magnetically confined wind-shock (MCWS) model. For checking Pollock's hypothesis, we determine the distribution of the ratio of half width at half maximum (HWHM) to the wind terminal velocity for lines in spectra of all examined stars. In addition, we check three probable consequences from the MCWS model. We analyze if a correlation exists between the spectral hardness and such stellar parameters as the wind terminal velocity, stellar magnetic field and mass loss rate. The result showed that Pollock's hypothesis is not correct. We also established that not all consequences of the MCWS model considered by us are confirmed. In addition, our spectral analysis method indicated that O stars probably have clumped stellar winds with spherical clumps.

Key words: stars: early-type — stars: spectra: X-ray

1 INTRODUCTION

Observations of stars in the Cygnus OB2 association by the *Einstein* space observatory led to the discovery that many early-type stars are bright X-ray sources (Harnden et al. 1979; Samus & Li 2018). However, there are some omissions in the theory of X-ray emission originating from O stars. The formation of X-ray emission from OB stars differs from that from low mass solar type stars. First of all, the generation of X-ray emission in OB stars is not connected only with their magnetic activity. There are principal reasons for this. Large-scale magnetism is not typical for all stars with radiative envelopes, so it cannot explain the presence of X-ray emission from most massive stars. Radiatively-driven winds of OB stars are orders of magnitude denser than those of solar-type stars. Massive stars have stellar winds with a temperature which is lower than the surface effective temperature (Drew 1989). OB stars that possess large-scale magnetic fields do not emit X-rays through the same coronal processes as low-mass stars do.

The most popular is an idea that the formation of X-ray emission from massive OB stars is tightly connected with their stellar winds. The first model of X-ray emission generated by stellar wind shocks was proposed by Lucy & White (1980). Feldmeier et al. (1997) developed a numerical radiative-hydrodynamic model of the X-ray emission from winds of an O star based on *ROSAT* observations. They suggested that X-rays are formed in the cooling zones behind shock fronts, where the cooling is primarily radiative. For magnetic OB stars, the formation of their X-ray emission can be described in the framework of the magnetically confined wind-shock (MCWS) model proposed by Babel & Montmerle (1997). In this model, matter that is part of the stellar wind moves along lines of the stellar magnetic field to the magnetic equator and collides there. The X-ray emission is produced in the post-shock region by hot plasma with low density. However, in case there is a weak magnetic field (weak magnetic pressure), only very weak winds could be confined.

In the MCWS model, matter that is part of the stellar wind moves mainly along the magnetic field lines.

We can propose the following possible consequences of this model. Firstly, due to the gravity darkening effect, the velocity of the wind depends on stellar latitude. For magnetic stars, this can lead to entanglement of magnetic field lines. Due to reconnection of the tangled field lines, hot plasma zones can appear. Cooling of these zones leads to an X-ray flash. The larger the magnetic field is, the larger the velocities of the charged particles appear due to reconnection. Larger velocities correspond to large plasma temperature heated by collisions of these particles. It means that the larger the stellar magnetic field is, the hotter these zones can be. These hot zones produce more hard X-ray emission, which means that the hardness of stellar X-ray spectra depends on the value of the stellar magnetic field and can be larger for stars with a larger magnetic field.

Secondly, stars with large mass loss rate have more dense matter in the region of the magnetic equator. Taking into account that the cooling function is much larger at $T \approx 10^6$ K than at $T \approx 10^7$ K (Sutherland & Dopita 1993) and remembering that the plasma cooling rate is proportional to the square of its density, we can conclude that the fraction of hot gas can grow if mass loss is enhanced. In this case, stars with bigger mass loss rate may have larger spectral hardness.

Thirdly, the temperature of hot gas in the region of the magnetic equator is larger for stars with high terminal wind velocity. This can mean that the largest hardness for X-ray spectra corresponds to stars with the fastest wind.

The question of whether the MCWS model is applicable to describe the X-ray emission of stars whose magnetic field has not yet been detected is unclear. It is possible that even in the case of a weak magnetic field, this model can also be applicable. Therefore, it would be interesting to investigate how well the above described consequences of the MCWS model can be applied to OB stars with a magnetic field that has not yet been detected.

In 2007, A. Pollock proposed his own hypothesis about the origin of X-ray emission from single O stars. He based it on the result of an analysis of X-ray observation of the supergiant ζ Ori (HD 37742) obtained in 2002 by the *XMM-Newton* satellite. Pollock made the following conclusions. In spectra of O stars, all lines have similar velocity profiles and all line profiles are broad and asymmetric. The X-ray emission of O stars is generated from the collisionless shocks in winds controlled by magnetic fields. The electron bremsstrahlung continuum is weak, and the emitting plasma is not in equilibrium. During post-shock relaxation, exchange of energy between ions and electrons is so slow that electron heating does not take place before hot gas is quenched by the majority of cool gas. Charge exchange, ionization and excitation can be realized by protons. Each observed line profile reflects the distribution of velocities of ions during the post-shock relaxation.

The shape of the observed line profiles according to Pollock reflects the line-of-sight component of the thermalized motion of ions in the immediate post-shock gas. In the case of a Maxwellian distribution, the half width at half maximum (HWHM) has to be the following (Pollock 2007)

$$\mathrm{HWHM} = \sqrt{2 \ln 2 \, (kT_\mathrm{S}/m)} \approx 0.51 v \,, \qquad (1)$$

where k is the Boltzmann constant, T_S is the post-shock gas temperature and m is the mean particle mass.

Apart from the above, it should be noted that in all aforementioned theories, X-ray spectra of O stars depend on more factors, such as stellar variability and stellar wind clumping. These correlations have been studied by Oskinova et al. (2006); Oskinova (2016); Oskinova et al. (2017). They demonstrated that shapes of X-ray emission spectral lines are related to stellar wind clumping and the form of clumps. In particular, if stellar wind is clumped, all X-ray emission lines should be nearly symmetric with similar shapes of the line profile. Authors modeled the line profiles for the clumped wind. If clumps are spherical, the X-ray emission lines should be skewed, but if clumps are slab-like then the line profiles should be symmetric. If stellar wind is smooth then the line profiles should be wide according to Oskinova et al. (2006). The X-ray line profiles are often variable. Variability of the X-ray line profiles can be associated with the changes in stellar wind structure and with stellar rotation. However, the reason for X-ray variability is not quite known yet.

In the present paper, we checked if Pollock's paradigm is true for O stars. We also consider three above mentioned consequences of the MCWS model both for magnetic and non-magnetic O stars. We have analyzed the archive of *XMM-Newton* X-ray observations for a sample of O stars and have compared our results with the public ones. The source of data and data reduction procedures are described in Section 2. In Section 3 we give our method of spectral parameter evaluation. The results of checking Pollock's hypothesis are presented in

Section 4. The possible consequences from the MCWS model are examined in Section 5. The final conclusions are given in Section 6.

2 OBSERVATION AND DATA REDUCTION

We analyzed the archival X-ray observations for 32 O stars. The list of studied stars and their parameters are given in Table 1. From the whole list of considered O type stars, four objects belong to the peculiar class Of?p, 15 stars are double or multiple, 17 stars are possible single and five stars have very strong lines relative to the continuum level in their X-ray spectrum.

The archive data we used were obtained by the *XMM-Newton* satellite in 2000–2014. The log of observations is given in Table 2. Data reduction was made following the recommendation given by the *XMM* team[1]. First of all, we filtered observations from background flares using the *tabgtigen* and *rgsfilter* SAS 14.0 tasks. Thereafter we extracted spectra by the *rgsproc* task and merged the stellar spectra of the first order of RGS1 and RGS2 in each set. We combined the spectra from different sets if stars were observed several times, using the *rgscombine* SAS 14.0 task. In the final spectra, we examined the wavelength interval from 6 to 40 Å. We used the AtomDB database[2] for line identification.

As an example in Figure 1 (top panel) we present the X-ray spectrum of the star HD 37742 (ζ Ori) with strong lines in its spectrum. The spectrum of HD 66811 with moderate intensity of spectral lines is displayed in the middle panel of Figure 1 and the spectrum of HD 148937 with weak spectral lines can be seen in the bottom panel.

3 SPECTRAL ANALYSIS

For checking the examined hypotheses, we have to identify lines in the X-ray spectra and estimate such line parameters as full width at half maximum (FWHM), ratio of HWHM to terminal velocity, HWHM/v_∞, maximum line flux for each line and spectral hardness. The last value is a ratio of maximum fluxes of ions in adjacent stages of ionization.

We used our own method for the line identification and for calculation of listed values. First of all, we have smoothed spectra with a narrow Gaussian filter. We selected the filter width $W = 0.01$ Å which is equal to the wavelength resolution of the Reflection Grating Spectrometer (RGS). Such a pipeline improved the signal-to-noise ratio without degrading the wavelength resolution. As a next step, we defined the boundaries of line profiles. We considered both isolated and blended line profiles which contain not less than 9–10 data points between the line boundaries (line edges). We assumed that up to four line profiles can be present inside each observed profile and up to five lines can be present in the case of wide profiles. Therefore, we fitted the observed line profiles by the sum of up to 4–5 components.

We consider two cases of the line profile fitting. In the first case, we present the blend as a sum of Gaussian-like functions

$$G_{\rm l}(\lambda) = \sum_{k=1}^{n} \frac{I_k}{\sqrt{2\pi}\,\sigma_k} \exp\left(-\frac{1}{2}\left(\frac{\lambda-\lambda_0^k}{\sigma_k}\right)^2\right), \quad (2)$$

where the amplitudes I_k, central line wavelengths λ_0^k and line widths σ_k are the parameters of the fitted profile of a line with a number k, and n is the total number of components in the blend. We consider the sum (2) both with common parameters $\sigma_k = \sigma$ for all lines and with different values of parameters σ_k.

In the second case, the observed line profile is a formula described as a sum of generalized Gaussians with variable power indexes

$$G_{\rm l}^{\alpha}(\lambda) = \sum_{k=1}^{n} \frac{I_k}{2^{1/\alpha_k}\Gamma(1/\alpha_k)\,\sigma_k} \exp\Big(-\frac{1}{2}\Big(\frac{\lambda-\lambda_0^k}{\sigma_k}\Big)^{\alpha_k}\Big). \quad (3)$$

Here $\alpha_k > 0$ is the fitting parameter for the line with a number k, and $\Gamma(x)$ is the gamma function of the argument x. Analogically to the first case, we can use this sum both with common parameters $\sigma_k = \sigma$ and with different values of σ_k for the various lines.

Furthermore, we used a linear approximation for the local continuum both for single and blended lines. The common line profile with a contribution of the local continuum can be presented as

$$G_{\rm l+c}(\lambda) = G_{\rm l}(\lambda) + G_{\rm c}(\lambda) = G_{\rm l}(\lambda) + C_1 + C_2\lambda, \quad (4)$$

or

$$G_{\rm l+c}^{\alpha}(\lambda) = G_{\rm l}^{\alpha}(\lambda) + G_{\rm c}^{\alpha}(\lambda) = G_{\rm l}^{\alpha}(\lambda) + C_1^{\alpha} + C_2^{\alpha}\lambda, \quad (5)$$

where C_1, C_2, C_1^{α} and C_2^{α} are the local continuum fitting parameters for these lines.

Examples of the line approximations in accordance with Equations (3) and (5) are given in Figure 2. One can

[1] *www.cosmos.esa.int/web/xmm-newton*

[2] *www.atomdb.org*

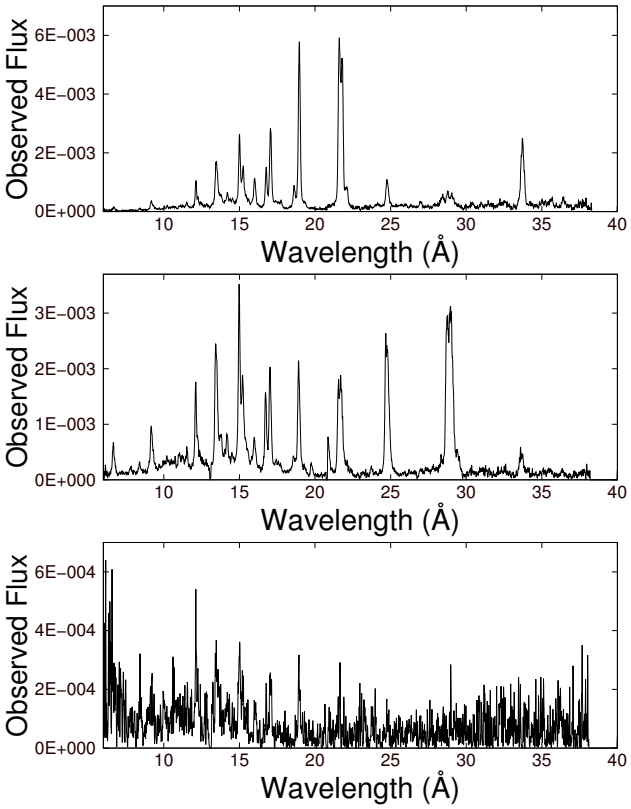

Fig. 1 X-ray spectrum of HD 37742 (*top panel*), HD 66811 (*middle panel*) and HD 148937 (*bottom panel*) which are smoothed with a narrow Gaussian filter ($W = 0.01$ Å).

see that the line profile in the spectral region $\lambda\lambda 11.30 - 11.38$ Å can be fitted with a different number of lines contributed to the observed profile. We can also see from an analysis of the figure that the larger the ionization potential of an ion, the smaller the width of the corresponding X-ray line.

We calculated the FWHM values (in km s^{-1}) for all lines in spectra of studied stars. In case an individual line profile can be approximated by a Gaussian function with parameters λ_0 and σ, we can use the standard expression

$$\mathrm{FWHM}_G = 2\sqrt{2\ln 2}\cdot\sigma\cdot\frac{c}{\lambda_0}. \quad (6)$$

For a generalized Gaussian function with a variable power α, we used the following expression for FWHM

$$\mathrm{FWHM}_G^{\alpha} = 2^{\frac{1+\alpha}{\alpha}}\cdot(\ln 2)^{\frac{1}{\alpha}}\cdot\sigma\cdot\frac{c}{\lambda_0}. \quad (7)$$

Here c is the speed of light in km s^{-1}. For all line profiles we checked the condition FWHM $< v_\infty$. In addition, for all line identifications we calculated the shift $\Delta\lambda = |\lambda_0^{\mathrm{fit}} - \lambda_0^{\mathrm{lab}}|$ between fitted and laboratory wavelength of the line. We used the condition $\Delta\lambda < 450$ km s^{-1}. This value is supposed to be the maximal possible line shift for lines which are formed in the stellar wind.

We determined the individual line contributions in all observed line profiles in spectra of the studied stars. Many of the profiles can be described by different approximations corresponding to the different cases of resolving multiple lines. We use only the approximations given by Equation (2) or Equation (3), for which the maximal difference between the observed and model line profiles does not exceed 10%.

In that way, we have defined the maximum and minimum possible numbers of individual lines that can be contributed into the observed profiles. The fluxes in the contributed lines were used to calculate the spectral hardness for different elements.

The values of FWHM for isolated lines contributed by 7–10 data points inside the line profile which cannot be approximated using formulae (2)-(7) were calculated by the next method. Firstly, we determine the equivalent width W of the line in Å by numerical integration. Secondly, supposing that the line profile may be

Table 1 The list of targets. The first column contains the star identifications. The spectral types of the stars are taken from the sources of terminal velocities, which are given in the notes below the table. The terminal velocity v_∞ of stars in km s^{-1} and references are presented in the third column and in the fourth column respectively. The last column includes some comments. In case there are no comments in the line, we suppose that the corresponding star is single.

Object	Spectral type	v_∞ (km s^{-1})	Reference	Note
CPD-282561	O6.5f?p	2400	f	
HD 108	O6f?p	1960	a	
HD 14947	O5If+	2350	j	Binary star
HD 15558	O4.5III(f)	2735	a	Binary star
HD 16691	O4If	2300	(m)	
HD 34078	O9.5V	800	b	Variable Star of Orion Type
HD 36861	O8 III ((f))	2175	a	Strong lines
HD 37468	O9.5V	1500	h	Binary star, strong lines
HD 37742	O9.7 Ib	2100	d	Binary or triple star, strong lines
HD 45314	O9:pe	2410	(k)	
HD 47129	O8I+O7.5III	3567	i	Binary star
HD 54662	O6.5 V	2456	a	Binary star
HD 57682	O9 IV	1200	e	
HD 60848	O8 V: per var	1765	a	
HD 66811	O4 I (n)f	2485	a	Variable of BY Dra type, strong lines
HD 93403	O5.5I+O7V	2615	a	Binary star
HD 93521	O9.5Vp	400	a	
HD 101205	O7 IIIn ((f))	2740	a	Binary star, eclipsing binary of β Lyr type
HD 113904	O9.5+WR	2255	a	Binary star
HD 148937	O6.5f?p	2600	c	
HD 152233	O6II(f)	2730	a	Binary star
HD 152248	O7Iabf+O7Ib(f)	2420	a	Binary star, eclipsing binary of β Lyr type
HD 152249	O9Ib((f))	2010	a	
HD 152408	O8: Ia fpe	955	a	
HD 155806	O7.5 V [n]e	2460	a	
HD 159176	O7 V((f))	2590	a	Binary star
HD 164794	O7.5III+O9.5III+O9.5	2750	a	Triple star, emission-line star
HD 167971	O8Iaf(n)+O4	2185	a	Binary star
HD 188001	O7.5 Ia f	1980	a	
HD 191612	O6f?p-O8fp	2700	g	
HD 210839	O6 I (n)fp	2300	a	
HD 215835	O6 V (n)	2810	a	Binary star

References for v_∞: (a) Howarth et al. (1997); (b) Martins et al. (2005); (c) Nazé et al. (2008); (d) Pollock (2007); (e) Grunhut et al. (2009); (f) Wade et al. (2015); (g) Sundqvist et al. (2012); (h) Najarro et al. (2011); (i) Nazé et al. (2014); (j) Repolust et al. (2004); (k) Vink et al. (2009); (m) Markova et al. (2005).

described by a Gaussian function, we use the following relation between the FWHM in km s^{-1} and W

$$\mathrm{FWHM} = 2\sqrt{\frac{\ln 2}{\pi}} \cdot \frac{W}{I} \cdot \frac{c}{\lambda_0}. \quad (8)$$

However, most of the line profiles of very strong lines that include more than 20 data points inside often have an irregular shape which could not be approximated with good precision. We fitted such profiles using formula (2) or (3) with a maximum error up to 30%. Upper limits of the fitting accuracy were determined experimentally by comparison with different line profile approximations.

The parameters of line approximations presented in Figure 2 are given in Table 3. We have determined, by the above mentioned method, the line parameters for all suitable lines in the 32 stellar spectra.

Parameters of the line profiles obtained by us were used for statistical analysis. We computed the ratios HWHM/v_∞ in percents and average FWHM value for each ion in the spectrum of all studied stars and ratios of

Table 2 Log of observations. In the first and fifth columns the object names are given. In columns (2) and (6) we put the observation ID numbers. Date of the observation and exposure in seconds are presented in columns (3), (7) and (4), (8) respectively.

Object	ObsID	Obs.date	Exp. (s)	Object	ObsID	Obs.date	Exp. (s)
(1)	(2)	(3)	(4)	(5)	(6)	(7)	(8)
CPD-282561	0740180501	04.05.2014	24000	HD 152233	109490101	05.09.2001	33870
	0740180601	14.05.2014	12999	HD 152248	109490201	06.09.2001	33773
HD 108	0109120101	21.08.2002	36685	HD 152249	109490301	07.09.2001	35009
HD 14947	0690880101	20.01.2013	21917		109490401	08.09.2001	31873
HD 15558	0740020101	25.08.2014	50000		109490501	09.09.2001	31664
HD 16 691	0671100101	21.08.2011	21719		109490601	10.09.2001	33505
HD 34078	0206360101	10.09.2004	58938				
HD 36861	0402050101	28.09.2006	56214	HD 152408	0602020101	30.08.2009	36914
HD 37468	101440301	23.03.2002	43820		0603570401	31.07.2009	33917
HD 37742	0657200101	03.09.2010	97810	HD 155806	0554440101	26.08.2008	36913
	0657200201	03.09.2011	47415		0561380601	08.10.2013	68800
	0657200301	29.08.2012	43912		0159360101	30.05.2003	72876
HD 45314	0670080301	14.04.2012	26226		0001730301	09.03.2001	9362
HD 47129	001730501	17.09.2002	21939		0001730401	09.03.2001	10859
	001730601	16.03.2003	21863				
HD 54662	0743660501	01.10.2014	33900	HD 159176	0001730201	09.03.2001	17083
HD 57682	0650320201	16.10.2010	11914	HD 164794	0720540401	08.03.2013	21916
HD 60848	0670080201	02.04.2012	32037		0720540501	03.09.2013	26700
HD 66811	0561380201	07.10.2010	76914		0720540601	05.03.2014	27500
HD 93403	0109530101	24.12.2000	10002	HD 167971	0740990101	09.09.2014	26800
	0109530201	28.12.2000	9817	HD 188001	0743660201	14.10.2014	33000
	0109530301	31.12.2000	9909		0740180701	30.05.2014	17900
	0109530501	31.12.2000	9211	HD 191612	0300600201	05.04.2005	28376
HD 93521	600620101	02.11.2009	41812		0300600301	02.06.2005	23813
HD 101205	0672060101	01.01.2012	41910		0300600401	08.10.2005	28915
HD 113904	0605670201	19.07.2009	54317		0300600501	17.04.2005	21775
HD 148937	022140101	25.02.2001	16507	HD 210839	0720090301	03.08.2013	77000
	022140501	25.02.2001	10531		0720090501	05.08.2013	96900
	022140601	25.02.2001	14610	HD 215835	0205650101	19.12.2003	31413

fluxes in the adjacent ionization stages in relative units (hardness value) for all considered stars. This allowed us to evaluate the ranges of spectral hardness by ions of the selected elements and the distribution function of the ratio HWHM/v_∞. Along with these, we have assessed the correlation between the average FWHM of different ions and their ionization potentials.

4 CHECKING POLLOCK'S PARADIGM

We analyzed the distribution of number of lines in different intervals for the ratio HWHM/v_∞. This distribution is presented in Figure 3 for the ratio HWHM/v_∞ ranging from 5% to 95%.

The first histogram (top-left panel) shows the result for all of 32 analyzed O stars, and the second (top-right panel) for single O stars. For double O stars and for O stars with strong lines in their spectra, the ratio HWHM/v_∞ is displayed in Figure 3 (middle-left and middle-right panels, respectively). Finally, we plot the numbers of lines in the selected intervals of the ratio HWHM/v_∞ for Of?p stars (bottom panel).

Examining Figure 3, we can conclude that most lines in spectra of examined stars have the ratio HWHM/v_∞ in the interval 5%–15%. This fact does not agree with Pollock's paradigm. In case his hypothesis is valid, most lines should be located in the interval 45%–55% of the HWHM/v_∞ ratio. The failure of Pollock's hypothesis may be explained by rapid cooling of hot gas behind the shock in the zone $v \approx v_\infty$. In this case, gas in the zone $v \approx v_\infty$ does not emit X-ray radiation. It also means that a bulk of the X-ray lines is formed close to the stellar surface where the gas velocity $v \ll v_\infty$.

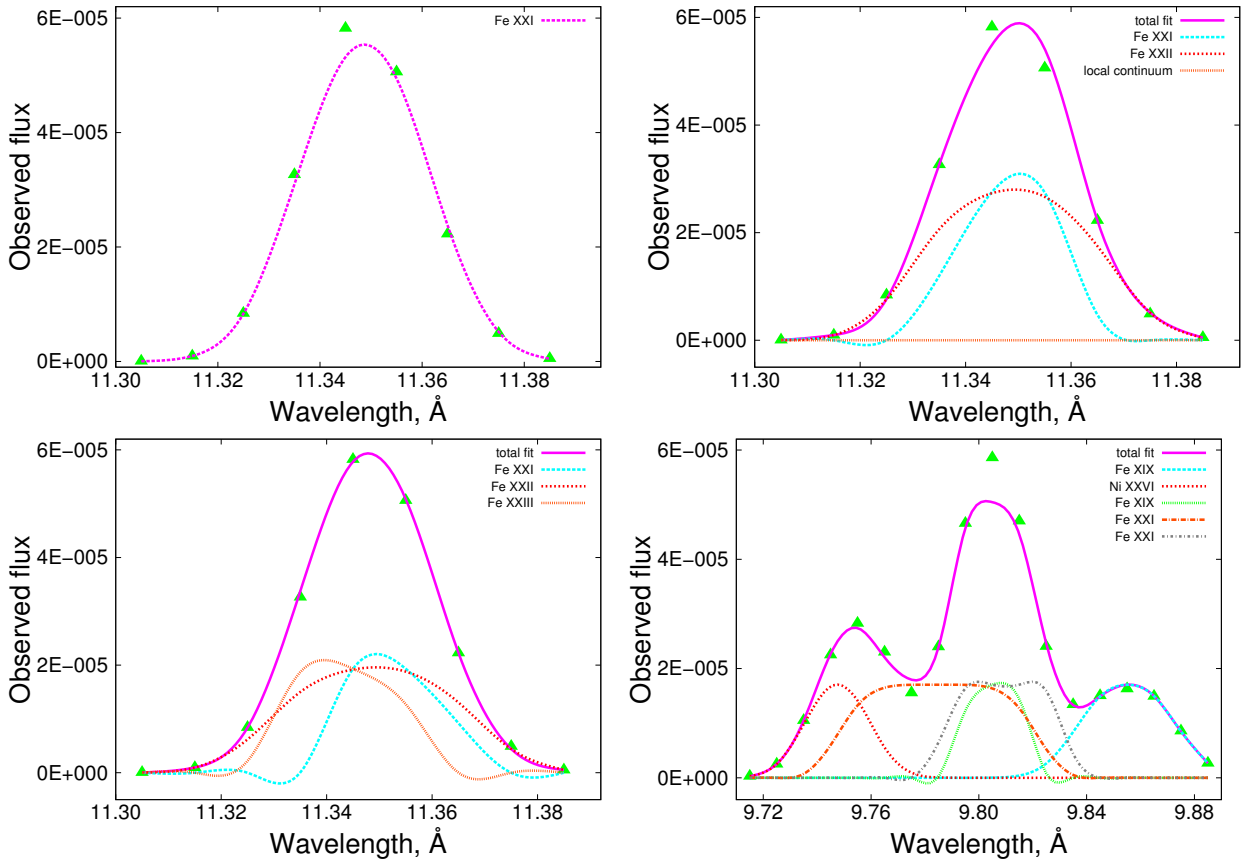

Fig. 2 Examples of blended resolution in spectra of HD 54662 near $\lambda = 11.25$ Å with one line (*top-left panel*), two lines (*top-right panel*), three lines (*bottom-left panel*) and in the region [9.715, 9.885] Å (*bottom-right panel*). Parameters of the line profiles contributed in the blends are given in Table 3.

5 CHECKING THE CONSEQUENCES OF THE MCWS MODEL

We have considered three possible consequences from the MCWS model, which were mentioned in the Introduction. To check these consequences, we estimated the spectral hardness for ions of iron and calcium. We chose the lines of these ions because they were detected in all stellar spectra investigated by us.

In the left panel of Figure 4, we show the dependence of spectral hardness on the magnetic field for all of the examined stars, whose magnetic fields are known. The list of these stars and values of their root mean square (rms) magnetic field are given in Table 4. In the right panel of Figure 4, we display the same dependence specially for OB stars. We can see only a marginal increase in the spectral hardness with enhancing value of the magnetic field.

In Figure 5 we present the dependence of the spectral hardness on the stellar mass loss both for all of the considered stars and for OB stars, all of which are magnetic. The list of stars with known mass loss rates is given in Table 4. Analyzing this figure, we can conclude that there is no dependence of the hardness on the mass loss both for magnetic and non-magnetic stars.

The relationship between spectral hardness and stellar terminal velocities both for all stars and for different types of stars is given in Figure 6. It appears that the mean hardness for the stars with large terminal velocities is slightly bigger than for those with small ones. There is no difference in the hardness vs. terminal velocity dependence both for magnetic and non-magnetic stars.

In addition, we have estimated the average value of FWHM for each ion in all examined spectra. Figure 7 (left) shows the dependence between the average FWHM of abundant ions and their ionization potentials in eV. The same dependence holds for less abundant ions. This plot demonstrates that the average FWHM enhances with the ionization potential linearly.

Table 3 Approximations of lines in the spectrum of HD 54662. First and second columns of the table give the short and long wavelength line edges. The third column lists the contributed ions. Line parameters of lambda, shift, FWHM and maximum value of flux are presented in the four following columns. Column (8) contains the biggest relative error of the fit. The formulas which were used to resolve the blend are given in Column (9). A label "num" means that the line parameters were detected using formula (8) without fitting the line profiles. The tenth column provides the number of lines contributed in the blend.

λ_1	λ_2	ion	λ_0	shift ($km\,s^{-1}$)	FWHM ($km\,s^{-1}$)	flux ($cm^{-2}\,s^{-1}\,Å^{-1}$)	err. (%)	exp.	cont.
(1)	(2)	(3)	(4)	(5)	(6)	(7)	(8)	(9)	(10)
7.805	7.885	Fe XXII	7.8650	0	1184	9.9190E–6	–	num	single
9.315	9.395	Ni XX	9.3650	32	749	2.2362E–5	–	num	single
11.305	11.385	Fe XXI	11.3487	7	175	5.7992E–5	7.6	$G_1^\alpha(\lambda)$	single
		Fe XXI	11.3491	–4	179	2.7566E–5	9.1	$G_{1+c}^\alpha(\lambda)$	double
		Fe XXII	11.3488	–20	456	2.7566E–5			
		Fe XXI	11.3517	–70	158	1.9320E–5	9.7	$G_1^\alpha(\lambda)$	triple
		Fe XXII	11.3488	–21	513	1.9320E–5			
		Fe XXIII	11.3425	–171	180	1.9320E–5			
		Fe XXI	11.3496	–14	219	4.6147E–5	6.1	$G_1^\alpha(\lambda)$	four
		Fe XXII	11.3481	–2	1233	2.2955E–7			
		Fe XX	11.3320	80	153	8.5712E–6			
		Fe XXIII	11.3581	208	461	7.3453E–6			
15.615	15.695	Fe XX	15.6342	14	1172	1.8692E–5	7.7	$G_1^\alpha(\lambda)$	double
		Fe XX	15.6527	101	318	1.8692E–5			
9.715	9.885	Ni XXVI	9.7558	–330	453	2.7586E–5	14.0	$G_1^\alpha(\lambda)$	triple
		Fe XIX	9.8024	263	295	5.0712E–5			
		Fe XIX	9.8410	334	1684	1.4632E–5			
		Fe XIX	9.8551	–2	587	1.7040E–5	15.5	$G_1^\alpha(\lambda)$	five
		Ni XXVI	9.7475	–78	160	1.7040E–5			
		Fe XIX	9.8059	157	152	1.7040E–5			
		Fe XXI	9.7845	–10	1676	1.7040E–5			
		Fe XXI	9.8093	295	801	1.7040E–5			
		Fe XIX	9.8515	156	886	1.6200E–5	15.2	$G_1^\alpha(\lambda)$	four
		Fe XXI	9.7680	398	2069	5.1123E–6			
		Fe XIX	9.8049	185	576	4.5645E–5			
		Ni XXVI	9.7559	–336	575	1.9165E–5			

In Figure 7 (right), the same dependence but on the binding energy in eV is shown. In this case, the dependence is more complicated. For ions of one element, the values of FWHM decrease with the binding energy, but each element demonstrates its own FWHM vs. binding energy dependence. The tables of ionization potentials and binding energies were taken from the ASD database[3].

6 DISCUSSION AND CONCLUSIONS

6.1 Line identification method

In the present paper, we used a simple approach for identification of spectral lines. We cannot determine the parameters for all lines because not all of them have a Gaussian-like shape. Moreover, our method can give different line contributions for many of the line profiles. For this reason, our statistical results are not completely unambiguous. It should also be noted that very strong lines can be either a sum of several Gaussian profiles with close line widths or they have a high local continuum level.

The result of line identification by our method demonstrates that most X-ray line profiles are narrow. For up to 70% of lines in spectra of the studied lines, a contribution of the local continuum is important. Many of the lines with a large contribution of the local continuum can be skewed. This can mean that these lines are formed in the clumped stellar wind from wind that

[3] *https://physics.nist.gov/PhysRefData/ASD/ionEnergy.html*

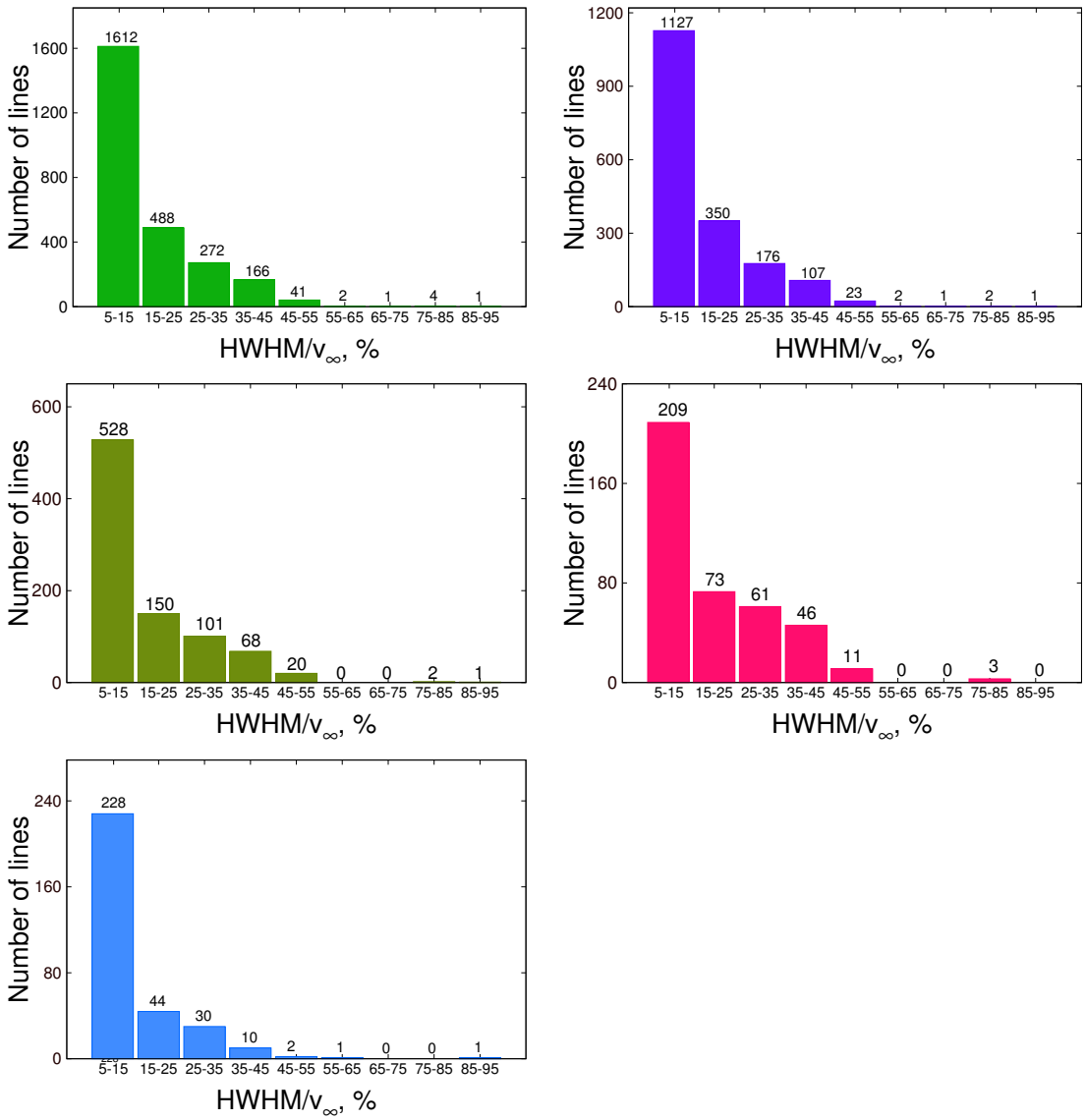

Fig. 3 *Top panel:* the distribution of HWHM/v_∞ ratios for all considered stars (*left*) and for single stars (*right*). *Middle panel:* the same as in the top panel but for double stars (*left*) and stars with strong lines in their spectra (*right*). *Bottom panel:* the same as in the top panel but for Of?p stars.

probably has spherical clumps according to the model by Oskinova et al. (2006).

6.2 Comments on the selected stars

6.2.1 HD 37742

The RGS spectrum of HD 37742 has the strongest observational line profiles. Many of them cannot be fit by Gaussian functions or Gaussian-like functions. So, we were able to identify only small lines in the spectrum of HD 37742. If we assume that lines with the biggest profiles are single, their FWHM would be more than the terminal velocity. Pollock (2007) determined spectral line parameters by the model "TriLine." In this model, he proposed that all strong lines are single but he did not take into account line blending so his conclusion is doubtful.

6.2.2 HD 113904

θ Muscae (WR 48, HD 113904) is known to be a complex object. It consists of an O type star and a Wolf-Rayet star, and probably an additional O supergiant companion. X-ray observation of HD 113904, which was applied

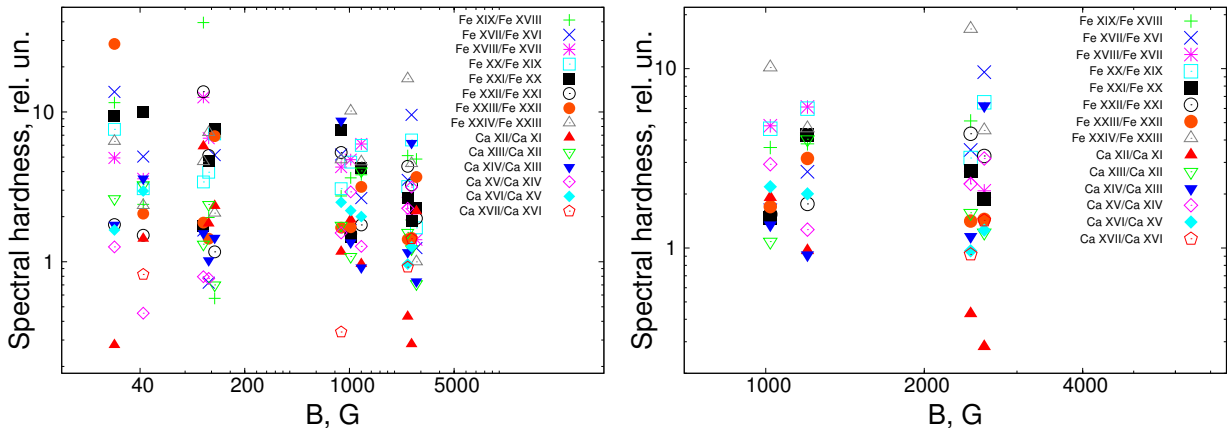

Fig. 4 *Left:* the spectral hardness vs. rms magnetic field for all stars. *Right:* the same as in the left panel but for Of?p stars.

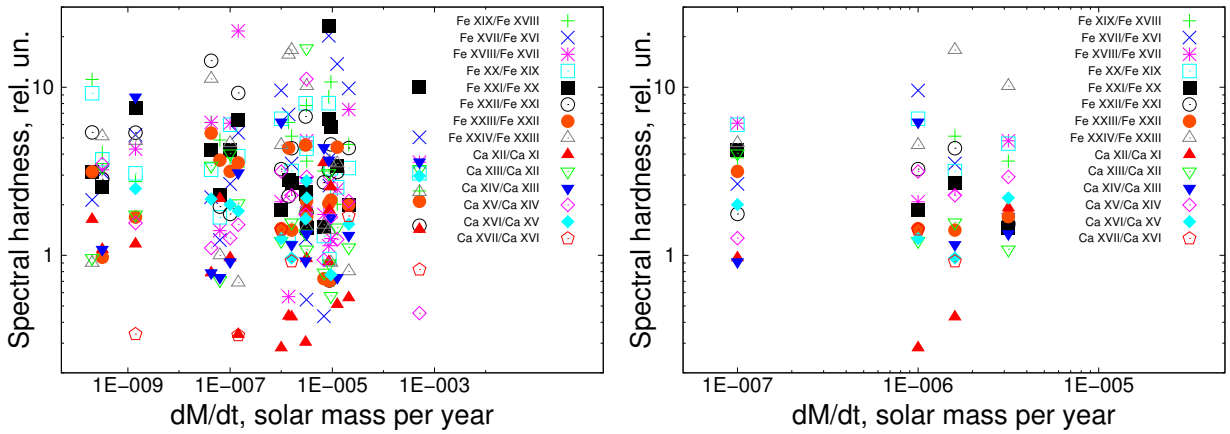

Fig. 5 *Left:* the spectral hardness vs. mass loss rates for all stars. *Right:* the same as in the left panel but for Of?p stars only.

in our work, was already analyzed by Sugawara et al. (2008). Their analysis did not confirm the scenario of the X-ray origin in the wind-wind collision zone associated with binary stars. These authors suggested that the collision zone is located behind the short-period binary.

6.2.3 HD 164794

This is a binary system with a long orbital period of 3324 days (Rauw et al. 2016). We used three sets of observations, which were obtained during the periastron passage in 2013. Rauw et al. (2016) analyzed these data and an additional observation from 2001 in detail. These authors did not reveal the short term variation of X-ray emission for HD 164794, but they suggested that X-ray emission undergoes a notable modulation during the orbital motion. The X-ray flux is highest at periastron as is expected for an adiabatic wind-interaction zone.

6.2.4 HD 188001

This object (9 Sge) was classified as a runaway star by Mason et al. (1998). In several papers, HD 188001 is considered as a binary system. For instance, Aslanov et al. (1984) ascertained that 9 Sge is an eclipsing binary with a period of 32.514 days. Underhill & Matthews (1995) proposed the presence of a compact companion for HD 188001. However, McSwain et al. (2007) did not confirm the binary nature of 9 Sge by spectroscopic observation. De Becker et al. (2017) analyzed the X-ray observation of HD 188001, but they did not mention multiplicity of this star. Therefore, in our work we assumed that HD 188001 is a single star.

6.2.5 HD 191612

This star was observed in the X-ray range by the *XMM-Newton* space observatory in 2005 and 2008, after HD

Table 4 Magnetic Field and Mass Loss Rates of Studied Stars

Object	B (G)	Reference	M ($M_\odot$ yr^{-1})	Reference
HD 108	1200	Martins et al. (2010)	1.0E–7	Martins et al. (2010)
HD 14947	–	–	8.52E–6	Repolust et al. (2004)
HD 16691	–	–	1.25E–05	Markova et al. (2005)
HD 34078	–	–	3.16E–10	Martins et al. (2005)
HD 37468	–	–	2.00E–10	Najarro et al. (2011)
HD 37742	–	–	1.40E–06	Pollock (2007)
HD 45314	–	–	4.27E–08	Vink et al. (2009)
HD 47129	–	–	6.31E–08	Nazé et al. (2014)
HD 57682	880	Grunhut et al. (2012)	1.41E–09	Grunhut et al. (2012)
HD 93403	42	Hubrig et al. (2011)	5.08E–04	Rauw et al. (2002)
HD 93521	126	Hubrig et al. (2013)	–	–
HD 148937	1020	Wade et al. (2012)	1.00E–07	Nazé et al. (2014)
HD 152233	106	Hubrig et al. (2011)	–	–
HD 152248	–	–	3.13E–06	Sana et al. (2004)
HD 152249	27	Hubrig et al. (2011)	–	–
HD 152408	–	–	2.10E–05	Prinja et al. (2001)
HD 155806	115	Hubrig et al. (2007)	–	
HD 159176	–	–	3.00E–06	
HD 167971	–	–	1.35E–06	
HD 191612	2450	Sundqvist et al. (2012)	1.60E–06	Sundqvist et al. (2012)
HD 210839	–	–	6.85E–06	Repolust et al. (2004)
CPD-282561	2600	Wade et al. (2015)	1.00E–06	Wade et al. (2015)

191612 was observed by the *Chandra* satellite in 2015–2016. All data were studied by Nazé et al. (2007, 2016). In both papers, authors showed that there are high- and low-emission states in stellar X-ray emission with a difference of about 40%. In our work we analyzed the X-ray spectrum of four *XMM-Newton* sets from 2005. There is no significant X-ray variability in such a spectrum, and these observational data demonstrated X-ray emission consistent with a "normal" O star (Nazé et al. 2007).

6.3 X-ray variability

X-ray emission short-time variability was revealed in some stars from our sample, i.e. HD 152248 (Sana et al. 2004), HD 93403 (Rauw et al. 2002), HD 191612 (Nazé et al. 2016), HD 167971 (De Becker 2015) and HD 101205 (Nazé et al. 2013b). But these variabilities have a small amplitude and not very short period. Nazé et al. (2013a) also showed that X-ray variability of O stars is not very strong. Therefore, we suppose that X-ray spectral lines in spectra, both of these stars and other studied stars, are not variable.

6.4 Pollock's paradigm

The results of our work demonstrate that Pollock's paradigm is not correct, but our conclusion is in agreement with the work Waldron & Cassinelli (2001) that many X-rays are produced mainly in dense regions very near the star. In addition, we have compared our distributions of the HWHM$/v_\infty$ ratios with analogical results of Waldron & Cassinelli (2007). Inasmuch as most stars considered by us belong to the main sequence, our result is consistent with their distributions with maximum ratios in the range 0–0.2.

In our previous work (Ryspaeva & Kholtygin 2017), we consider only single lines. We proposed that all observed line profiles have Gaussian-like forms and correspond to single profiles; their parameters were calculated by the numerical method without approximation. The results of this paper are similar to those obtained in the present paper. Considering not only single but also blended lines does not challenge the conclusion by Ryspaeva & Kholtygin (2017) that Pollock's paradigm is incorrect.

6.5 MCWS model

The consequences of the MCWS model supposed by us can only marginally be confirmed from our study of the X-ray spectra of O stars. It should be mentioned that the MCWS model was developed only for magnetic stars. As can be seen from the plots for magnetic Of?p stars in

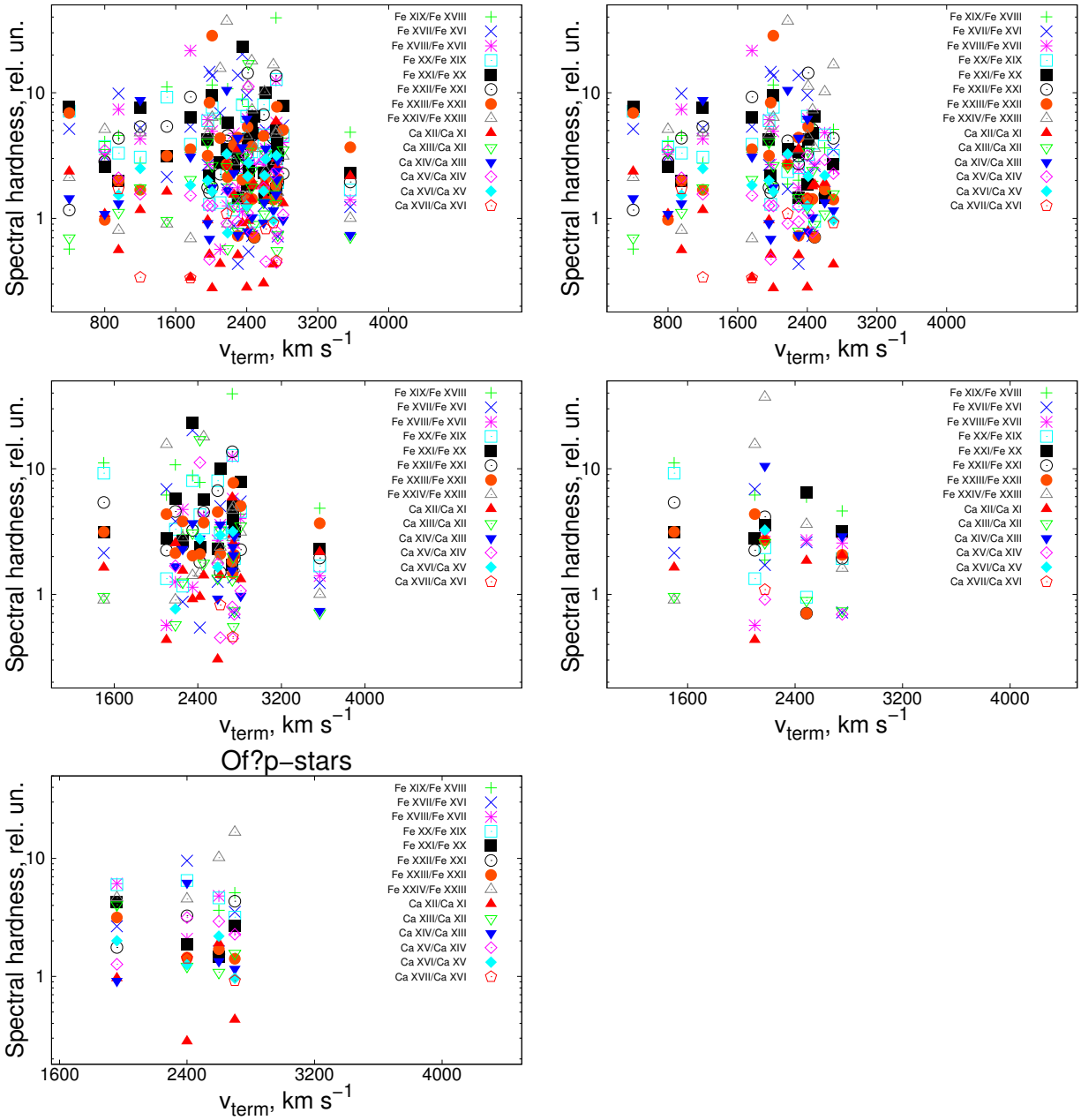

Fig. 6 *Top panels:* the dependence on spectral hardness of the wind terminal velocity for all considered stars (*left*) and for single stars (*right*). *Middle panels:* the same as in the top panels but for double stars (*left*) and stars with strong lines in their spectra (*right*). *Bottom panel:* the same as in the top panels but for OB stars.

Figures 5 and 6, the relationships of spectral hardness on the terminal velocity and mass loss rate differ a little from the analogical ones for all other target stars. However, we cannot exclude the difference in parameters in X-ray spectra of magnetic and non-magnetic O stars.

Mass loss rates and magnetic field values are known only for a few O stars and not all of them were observed in the X-ray range, which means that it would be very important to acquire more X-ray spectra of O stars to establish if a correlation exists between the values considered by us and the X-ray spectral hardness.

7 GENERAL CONCLUSIONS

Based on our analysis of the X-ray spectra of 32 O stars, we can make the following conclusions:

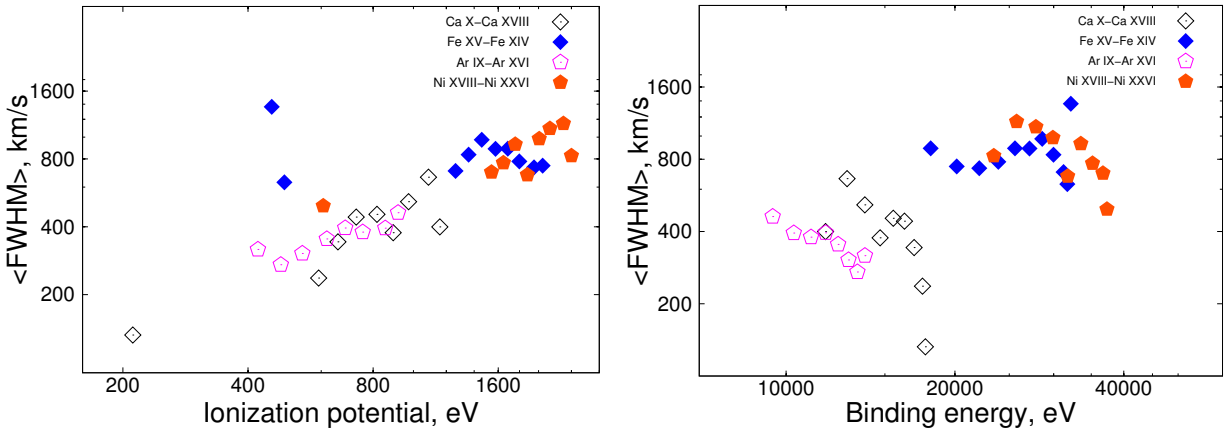

Fig. 7 *Left:* the dependence of the average FWHM of spectral lines on ionization potential for all groups of studied stars. *Right:* the dependence of the average FWHM of spectral lines on total ionization potential for all groups of studied stars.

(1) The most probable value of the ratio of HWHM for lines in spectra of all considered stars to the wind terminal velocity v_∞ is in the interval from 0.05–0.15. It contradicts the Pollock (2007) paradigm of the formation of X-ray spectra for O stars. We conclude that the X-ray emissions originate mainly from regions close to the stellar surface.

(2) We analyzed possible consequences of the MCWS model. We established that not all consequences from the MCWS model considered by us are confirmed. In particular, the spectral hardness does not depend on the mass loss rate for all of the studied O stars. Spectral hardness most probably decreases with an increasing stellar magnetic field. Spectral hardness increases first, then decreases with terminal velocity. It can also mean that X-ray emission is formed close to the star.

(3) We analyzed the shape of line profiles in all spectra. The majority of lines has skewed profiles and these lines are not wide. This means that O stars considered by us have clumped stellar winds with spherical clumps.

(4) We reveal the enhancement of HWHM with ion ionization potential and the decrease of this value with binding energy. This does not contradict our conclusion that the bulk of X-ray emission is formed close to the star.

Acknowledgements This study was carried out with support from the Russian Science Foundation project No. 18-12-00423. ER is also grateful to RFBR grant 18-02-00554.

References

Aslanov, A. A., Kornilova, L. N., & Cherepashchuk, A. M. 1984, Soviet Astronomy Letters, 10, 278
Babel, J., & Montmerle, T. 1997, A&A, 323, 121
De Becker, M. 2015, MNRAS, 451, 1070
De Becker, M., del Valle, M. V., Romero, G. E., Peri, C. S., & Benaglia, P. 2017, MNRAS, 471, 4452
Drew, J. E. 1989, ApJS, 71, 267
Feldmeier, A., Kudritzki, R.-P., Palsa, R., Pauldrach, A. W. A., & Puls, J. 1997, A&A, 320, 899
Grunhut, J. H., Wade, G. A., Marcolino, W. L. F., et al. 2009, MNRAS, 400, L94
Grunhut, J. H., Wade, G. A., Sundqvist, J. O., et al. 2012, MNRAS, 426, 2208
Harnden, Jr., F. R., Branduardi, G., Elvis, M., et al. 1979, ApJ, 234, L51
Howarth, I. D., Siebert, K. W., Hussain, G. A. J., & Prinja, R. K. 1997, MNRAS, 284, 265
Hubrig, S., Yudin, R. V., Pogodin, M., Schöller, M., & Peters, G. J. 2007, Astronomische Nachrichten, 328, 1133
Hubrig, S., Schöller, M., Kharchenko, N. V., et al. 2011, A&A, 528, A151
Hubrig, S., Schöller, M., Ilyin, I., et al. 2013, A&A, 551, A33
Lucy, L. B., & White, R. L. 1980, ApJ, 241, 300
Markova, N., Puls, J., Scuderi, S., & Markov, H. 2005, A&A, 440, 1133
Martins, F., Schaerer, D., Hillier, D. J., et al. 2005, A&A, 441, 735
Martins, F., Donati, J.-F., Marcolino, W. L. F., et al. 2010, MNRAS, 407, 1423
Mason, B. D., Gies, D. R., Hartkopf, W. I., et al. 1998, AJ, 115, 821
McSwain, M. V., Boyajian, T. S., Grundstrom, E. D., & Gies, D. R. 2007, ApJ, 655, 473
Najarro, F., Hanson, M. M., & Puls, J. 2011, A&A, 535, A32

Nazé, Y., Rauw, G., Pollock, A. M. T., Walborn, N. R., & Howarth, I. D. 2007, MNRAS, 375, 145
Nazé, Y., Walborn, N. R., Rauw, G., et al. 2008, AJ, 135, 1946
Nazé, Y., Oskinova, L. M., & Gosset, E. 2013a, ApJ, 763, 143
Nazé, Y., Rauw, G., Sana, H., & Corcoran, M. F. 2013b, A&A, 555, A83
Nazé, Y., Petit, V., Rinbrand, M., et al. 2014, ApJS, 215, 10
Nazé, Y., ud-Doula, A., & Zhekov, S. A. 2016, ApJ, 831, 138
Oskinova, L. M., Feldmeier, A., & Hamann, W.-R. 2006, MNRAS, 372, 313
Oskinova, L. M. 2016, Advances in Space Research, 58, 739
Oskinova, L. M., Ignace, R., & Huenemoerder, D. P. 2017, in IAU Symposium, 329, The Lives and Death-Throes of Massive Stars, ed. J. J. Eldridge, J. C. Bray, L. A. S. McClelland, & L. Xiao, 151
Pollock, A. M. T. 2007, A&A, 463, 1111
Prinja, R. K., Stahl, O., Kaufer, A., et al. 2001, A&A, 367, 891
Rauw, G., Vreux, J.-M., Stevens, I. R., et al. 2002, A&A, 388, 552
Rauw, G., Blomme, R., Nazé, Y., et al. 2016, A&A, 589, A121
Repolust, T., Puls, J., & Herrero, A. 2004, A&A, 415, 349
Ryspaeva, E. B., & Kholtygin, A. F. 2017, Astronomische Nachrichten, 338, 959
Sana, H., Stevens, I. R., Gosset, E., Rauw, G., & Vreux, J.-M. 2004, MNRAS, 350, 809
Samus, N. N., & Li, Y., RAA (Research in Astronomy and Astrophysics), 2018, 18, 88
Sugawara, Y., Tsuboi, Y., & Maeda, Y. 2008, A&A, 490, 259
Sundqvist, J. O., ud-Doula, A., Owocki, S. P., et al. 2012, MNRAS, 423, L21
Sutherland, R. S., & Dopita, M. A. 1993, ApJS, 88, 253
Underhill, A. B., & Matthews, J. M. 1995, PASP, 107, 513
Vink, J. S., Davies B., Harries, T. J. et al., 2009, A&A, 505, 743
Wade, G. A., Grunhut, J., Gräfener, G., et al. 2012, MNRAS, 419, 2459
Wade, G. A., Barbá, R. H., Grunhut, J., et al. 2015, MNRAS, 447, 2551
Waldron, W. L., & Cassinelli, J. P. 2001, ApJ, 548, L45
Waldron, W. L., & Cassinelli, J. P. 2007, ApJ, 668, 456